Peeling studies as a proxy for understanding fracture mechanics and other interesting phenomena

Chiraag Nataraj

June 5, 2015

Contents

Chapter 1

Introduction

1.1 Background

Fracture mechanics is an extremely important area in the field of solid mechanics. Fracture mechanics concerns itself with the creation, propagation, and evolution of cracks in materials. It is an significant field due to the importance fracture of materials plays in many areas. In many settings, knowing how to detect and mitigate failure of materials (i.e. fracturing) can be the difference between no loss of life and hundreds of lives lost, the difference between predictable (and therefore manageable) failure and unpredictable and catastrophic failure.

The fracture mechanics of homogeneous materials is well understood. There has been a great amount of work put in to understanding, both theoretically and practically, the mechanics behind both initial fracturing as well as how the crack propagates through the material. A general theory to deal with any kind of homogeneous material has been fairly well established, leading to all of the advances in obtaining desired material properties that we see today.

Homogeneous materials, however, can only get us so far. The future advances in material properties will come from heterogeneous materials. However, there is an issue: unlike with homogeneous materials, there is no one unifying theory describing all heterogeneous materi-

als. It is therefore difficult to design a material with specific properties in mind without first having a generalized model of all such materials with modifiable parameters. This is exactly why homogeneous materials have been so successful in this arena. In addition, it would be great to be able to model *any* heterogeneous material. It would increase our knowledge about the world and possibly open up new avenues for exploration.

Moreover, even supposed homogeneous materials are not truly homogeneous — there are always cracks, bumps, dents, and other deformities. For example, it is easier to rip paper or cardboard in one direction than in the other due to the way the fibers are aligned. Additionally, heterogeneity is built-in to the microstructure of many materials, such as metallic and ceramic materials. Thus, studying the fracture mechanics of macroscopically heterogeneous materials will *also* benefit the modeling of many common-place materials which are homogeneous at our length scales, but heterogeneous at smaller length scales.

1.2 Objectives

In order to study the fracture mechanics of heterogeneous materials as an avenue for attempting to characterize heterogeneous materials, it is useful to utilize alternative measures which are easier to measure while providing an understanding of the underlying phenomena. The behavior of heterogeneous materials under peeling action will be explored as a proxy for understanding fracture mechanics.

The first objective is to perform a peeling experiment to investigate how different patterns on a substrate affect adhesion. Several different patterns will be tested and the force required to peel the tape off at constant velocity will be measured. I will attempt to mathematically model the results from that experiment as well as design further experiments to test hypotheses about phenomena that may arise.

The second objective is to computationally model the peel front during the peeling process

to track how it changes. This will thus give an idea of how the heterogeneities affect the peel front.

1.3 Thin-Film Peeling

Front propagation problems are of paramount importance in areas such as phase boundaries [1, 2, 3] and crack propagation [4, 5]. As the underlying mathematics of front propagation problems is similar to that of thin-film peeling, the latter can be used as a model system for the former.

This problem was first explored analytically by Rivlin (1944) [6]. The thin-film peeling problem is often modeled as either a membrane or Euler-Bernoulli beam. The peeling angle is held constant and the resulting peel front examined.

Most of the following is taken from [8]. In order to derive the theoretical foundation for the analytical part of this research, it is necessary to start with Kirchoff finite deformation theory. One then makes a Kirchoff-Love hypothesis and assumes the peel front has a two-scale form. One then does a Taylor expansion to finish dealing with scale.

One then computes the first variation of the potential energy expression to obtain the governing equations (letting $G_\infty = \frac{D}{2}\left(\kappa^0\right)^2$):

$$\Delta^2 w = 0 \tag{1.1}$$

$$G \approx G_\infty + D\kappa^0 w_{,11} \tag{1.2}$$

$$G = G_c\left(\dot{f}, x_1, x_2\right) \tag{1.3}$$

One then solves Equation (1.1) by separation of variables and gets:

$$W_k(x_1) = \kappa^0 x_1 \exp(-|k| x_1) \hat{f}(k) \tag{1.4}$$

It is evident from Equation (1.2) that the Fourier transform of the energy release rate is:

$$\hat{G}(k) = 2\pi G_\infty \delta(k) + 2D\left(\kappa^0\right)^2 |k| \hat{f} \tag{1.5}$$

$$= G_\infty \left(2\pi - 4|k| \hat{f}\right) \tag{1.6}$$

Taking the inverse Fourier transform of Equation (1.6) yields:

$$G(x_1) = G_\infty - \frac{4G_\infty}{\pi} PV \int_{-\infty}^{\infty} \frac{f(\xi) - f(x_1)}{(\xi - x_1)^2} d\xi \tag{1.7}$$

where PV is the principal value of the integral. Given that the critical energy release rate is linear in the velocity, we can write:

$$G_\infty \left(2\pi - 4|k| \hat{f}\right) = \mathcal{F}\left(G_c^0(x_1, f(x_1))\right) + \mu \dot{\hat{f}} \tag{1.8}$$

Here, we diverge slightly from [8]. We can now take this equation and discretize it in time (taking $\mu = 1$):

$$\dot{\hat{f}} = G_\infty \left(2\pi - 4\left|k\right|\hat{f}\right) - \mathcal{F}\left(G_c^0\left(x_1, f\left(x_1\right)\right)\right) \tag{1.9}$$

$$\frac{\hat{f}^{[n+1]} - \hat{f}^{[n]}}{\Delta t} = -4G_\infty \left|k\right| \hat{f}^{[n]} + \mathcal{F}\left(\left[G_\infty - G_c^0\left(x_1, f\left(x_1\right)\right)\right]^{[n]}\right) \tag{1.10}$$

$$\hat{f}^{[n+1]} = \hat{f}^{[n]} + \Delta t \left(-4G_\infty \left|k\right| \hat{f}^{[n]} + \mathcal{F}\left(\left[G_\infty - G_c^0\left(x_1, f\left(x_1\right)\right)\right]^{[n]}\right)\right) \tag{1.11}$$

Equation (1.11) is the update rule given the previous timestep's peel front.

Chapter 2

Methods

There are two main components to this exploration of fracture mechanics of heterogeneous materials. The first is a series of experiments that explores how different patterns affect adhesion. The second is a computational exploration of the history of the peel front when confronted with different patterns.

2.1 Experiment

The main premise of the experiment has been described above. The objective of the experiment is to investigate how different patterns on a substrate affect adhesion. To this end, the following experiment has been designed, based heavily off of the experiment used in [8].

2.1.1 Preparation

The first issue at hand is to select the patterns to test. After deliberating for some time, the following patterns were chosen: horizontal, vertical, $\pm 30°$, $\pm 45°$, $\pm 60°$, and semicircles ranging from $0°$ to $270°$ (see Figures 2.1 to 2.6).

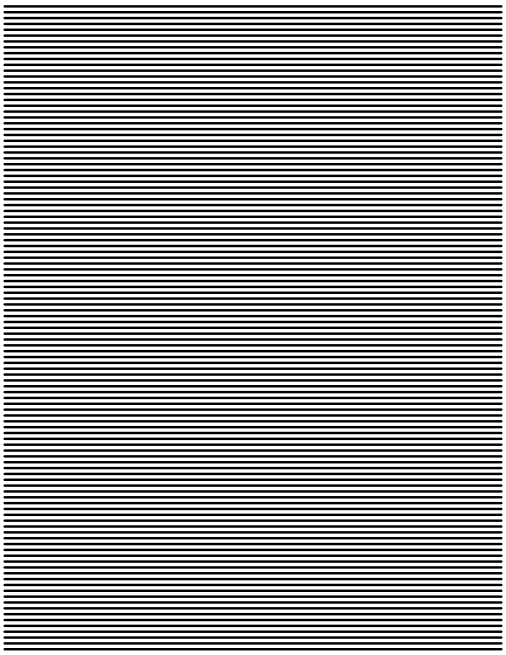

Figure 2.1: Horizontal Pattern

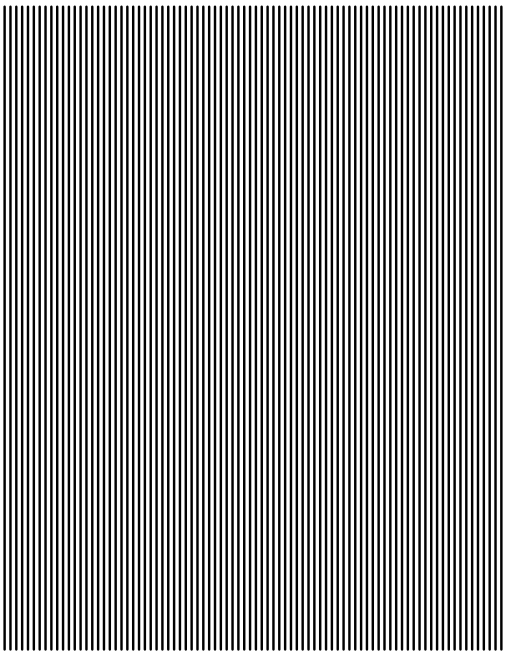

Figure 2.2: Vertical Pattern

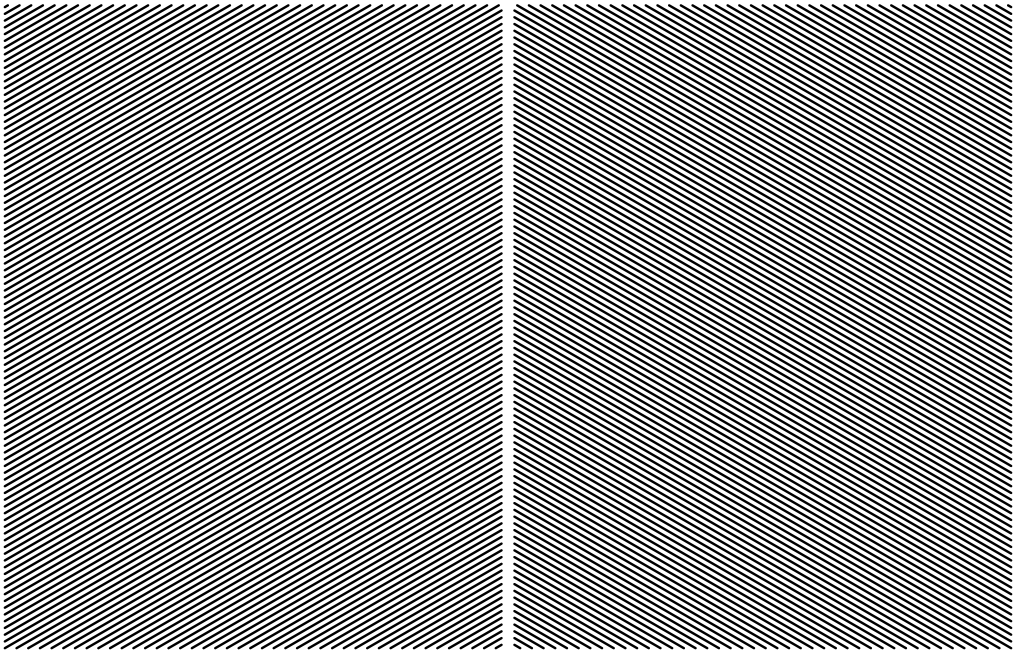

(a) 30° Angled Pattern (b) -30° Angled Pattern

Figure 2.3: ±30° Patterns

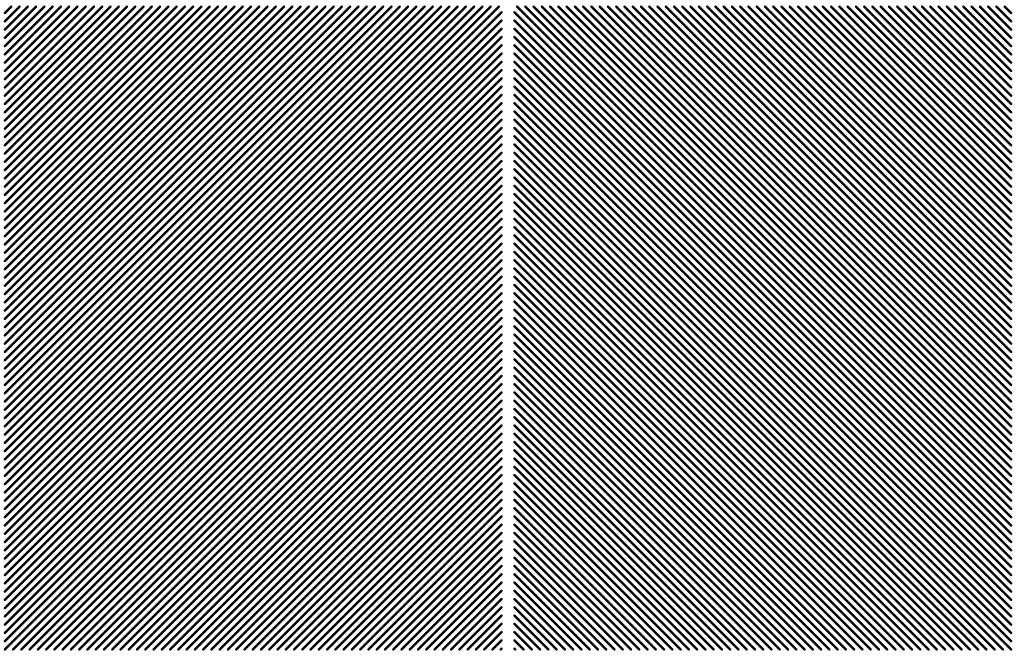

(a) 45° Angled Pattern (b) -45° Angled Pattern

Figure 2.4: ±45° Patterns

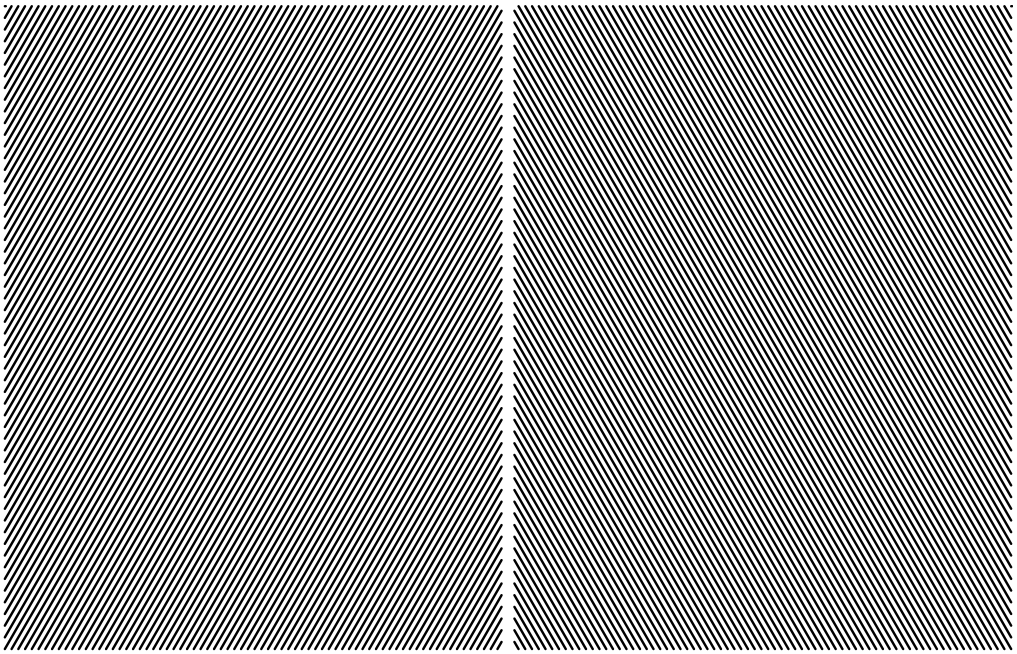

(a) 60° Angled Pattern (b) -60° Angled Pattern

Figure 2.5: ±60° Patterns

2.1.2 Peel Testing

The experiment itself is fairly straightforward. The patterned substrate is mounted on a flat table (to keep the peel angle relatively constant). The film is peeled off of the substrate at a constant peel speed using a vertically mounted linear stage (see Figure 2.8).

2.1.3 Data

The data which will be analyzed is the force history. Using a DAQ, LabView, and a load cell, it is quite easy to gather the data.

2.1.4 Procedure

1. Initialize
    - Start-up load cell (but don't collect data yet)

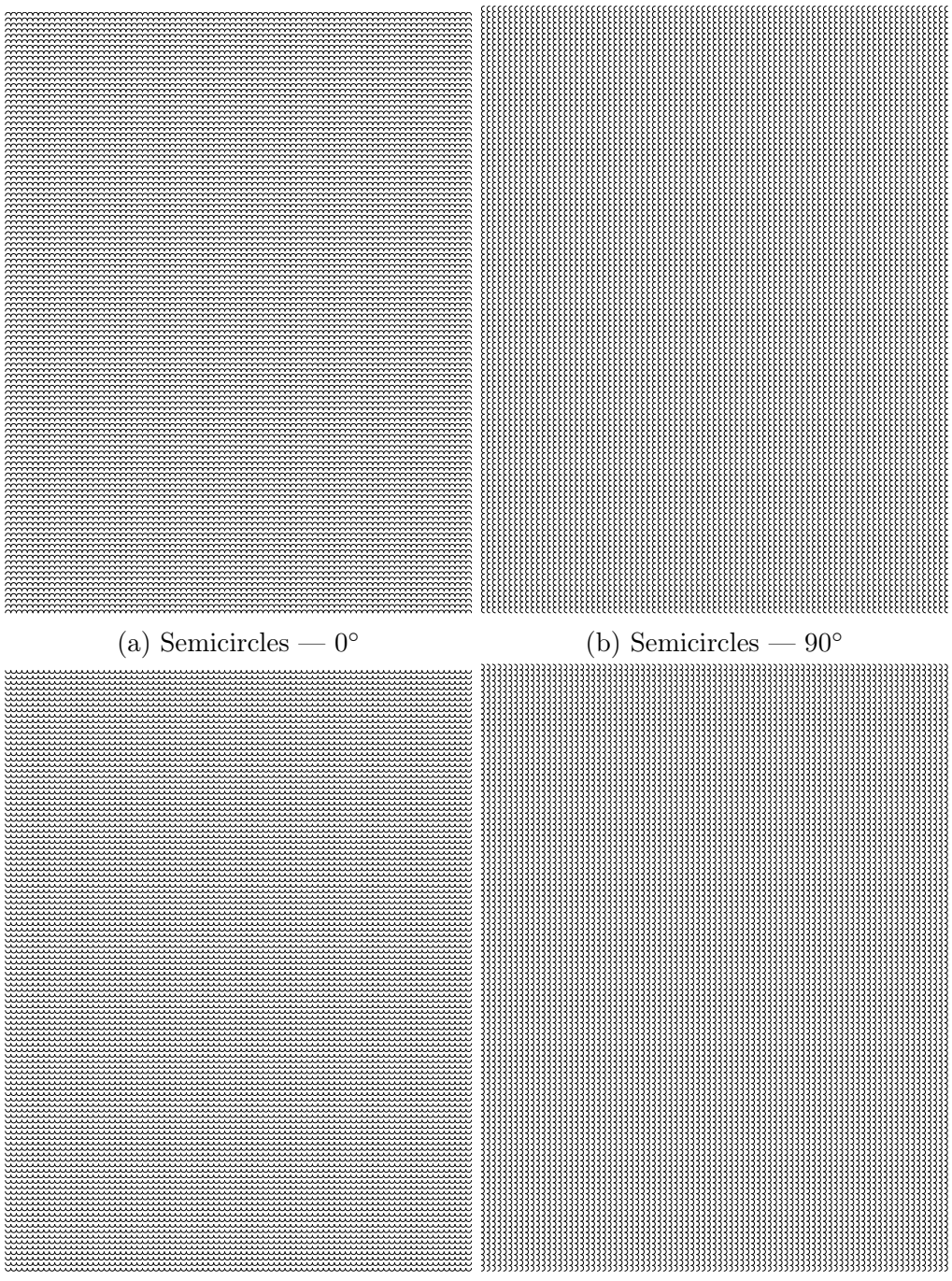

(a) Semicircles — 0°

(b) Semicircles — 90°

(c) Semicircles — 180°

(d) Semicircles — 270°

Figure 2.6: Curved Patterns

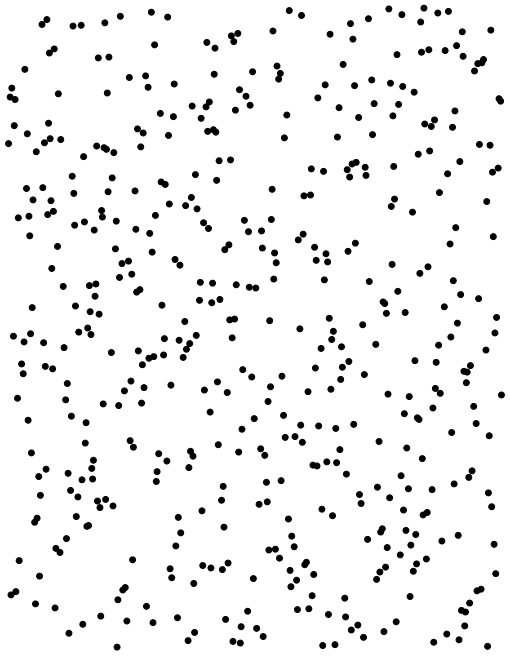

Figure 2.7: Random Pattern

- Move stage to 90 mm
- Attach pattern to substrate using double-sided tape
- Setup (normal) tape in peel test initial configuration

2. Run
   - Restart the load cell (and start collecting data)
   - Turn on stage motor to raise stage to 100 mm at a rate of 0.1 $^{\text{mm}}/_{\text{s}}$
3. End data collection once the stage reaches 100 mm

2.1.5 Control

In order for the data collected in Section 2.1.3 to make any sense, there needs to be a baseline. The baseline is the force required to peel tape off of an unpatterned substrate. This measurement allows the data collected from the experiment to be interpreted properly.

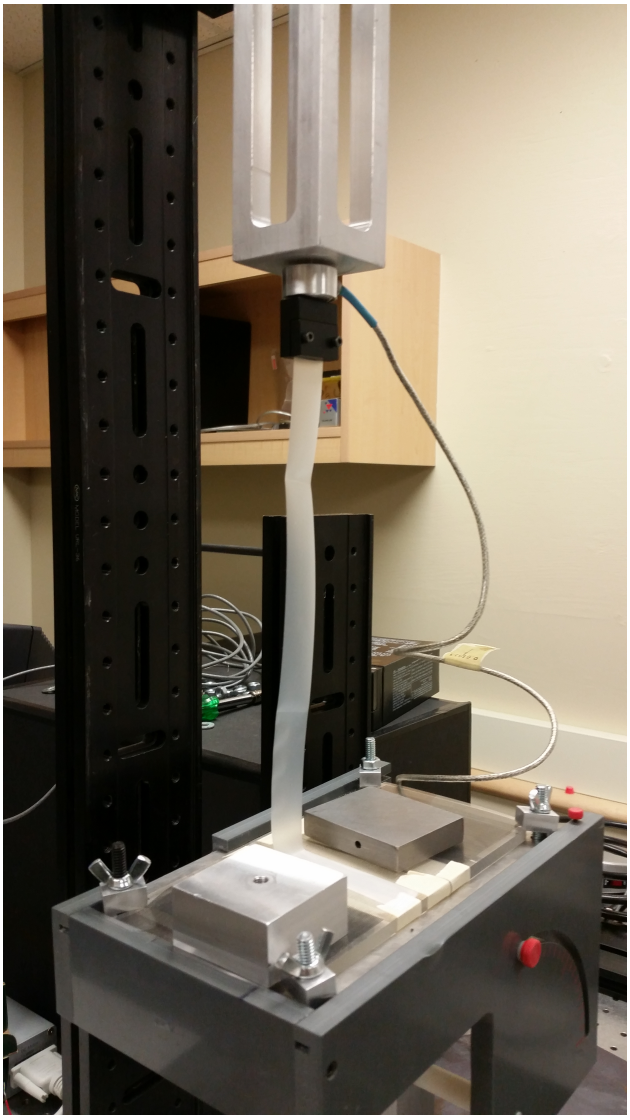

Figure 2.8: Experiment setup

2.2 Analytical Methods

The conventions followed throughout this thesis are as follows. Functions are notated as $f(x,t)$, while Fourier Transforms of functions are notated as $\hat{f}(k,t)$ and alternatively as $\mathcal{F}(f)$.

In studying thin film peeling analytically, the object of interest is the peel front — if one can characterize that, one knows the precise shape of the thin film over time and space, which provides detailed information about the shape of the film and thus information about how the irregularities in the substrate affect the peeling process.

In order to characterize the peeling process, let us first define the peel front as $y = f(x,t)$. The dimensions of the substrate are $L \times L$. Let us now define the locations of irregularities in the substrate (the part that makes the substrate heterogeneous) using a function $G(x,y)$. Initially, $G(x,y)$ will be periodic in both x and y, but that can (and will) change.

Now, to find how the peel front varies over time, we can write Equation (2.1). However, this is much more convenient to work with if we work in Fourier space, thereby yielding Equation (2.2).

When specifying a problem, we know $G(x,y)$ and we know $f(x,0)$ (i.e. the initial condition of the peel front). In order to solve this numerically, we can set up a finite difference scheme. We discretize the time derivative using a Forward Euler scheme, yielding Equation (2.3), where $\hat{f}^n = \hat{f}(k,t_n)$. This can now be implemented using various $G(x,f(x,t))$ to study the evolution of the peel front.

$$\frac{\partial f}{\partial t}(x,t) = c\int_{-\infty}^{\infty} \frac{f(\xi,t)}{|x-\xi|}\,d\xi + G_\infty - G(x,f(x,t)) \tag{2.1}$$

$$\frac{\partial \hat{f}}{\partial t}(k,t) = -c|k|\,\hat{f}(k,t) + \mathcal{F}\left[G_\infty - G(x,f(x,t))\right] \tag{2.2}$$

$$\frac{\hat{f}^{n+1} - \hat{f}^{n}}{\Delta t} = -c\,|k|\,\hat{f}^{n} + \mathcal{F}\left[G_{\infty} - G\left(x, f\left(x,t\right)\right)\right]^{n} \tag{2.3}$$

Chapter 3

Results

3.1 Experimental Results

3.1.1 Results

Homogeneous

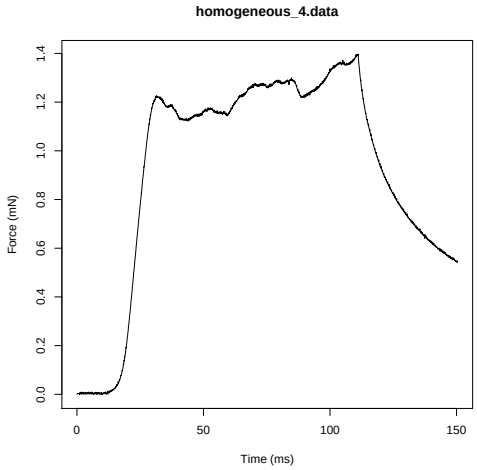

Figure 3.1: Homogeneous Trial 1

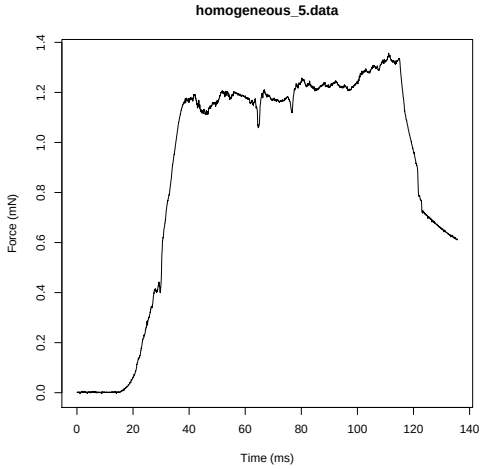

Figure 3.2: Homogeneous Trial 2

Horizontal Pattern

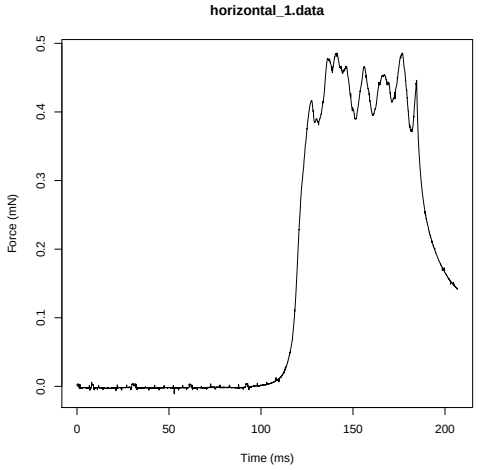

Figure 3.3: Horizontal Pattern Trial 1

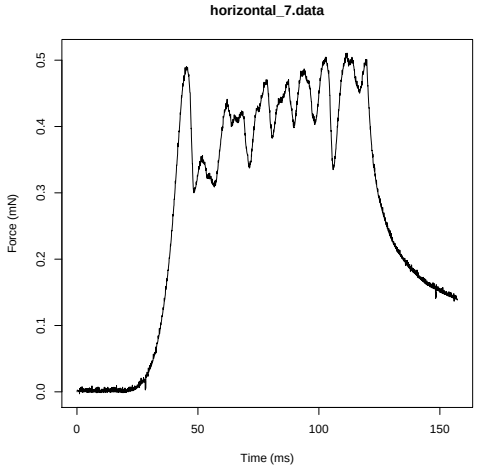

Figure 3.4: Horizontal Pattern Trial 2

Vertical Pattern

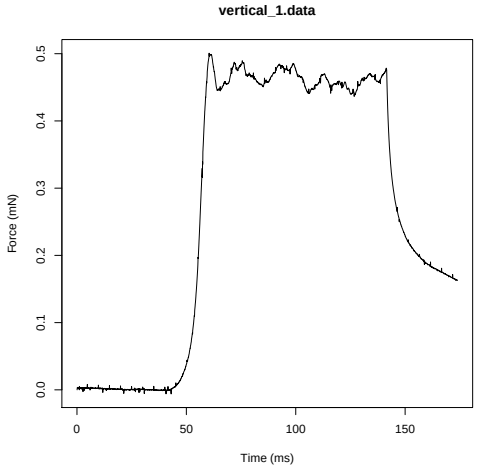

Figure 3.5: Vertical Pattern Trial 1

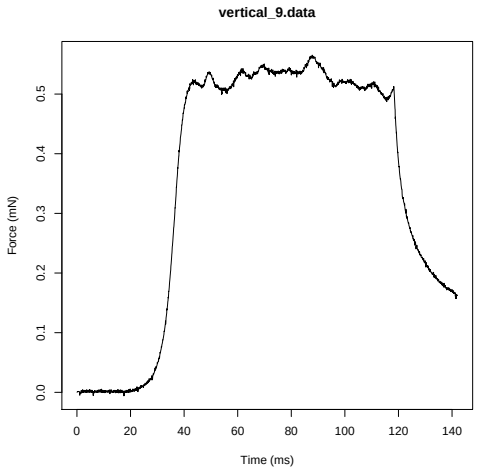

Figure 3.6: Vertical Pattern Trial 2

Angled Patterns

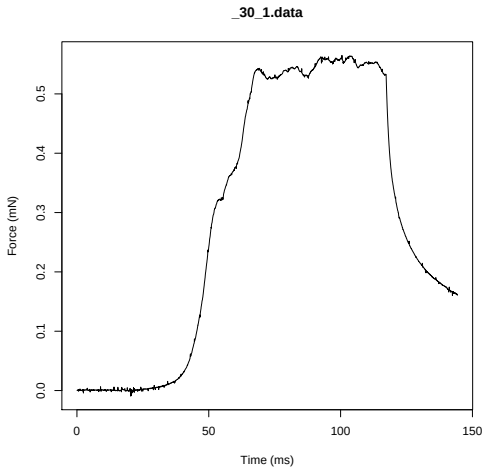

Figure 3.7: $-30°$ Pattern Trial 1

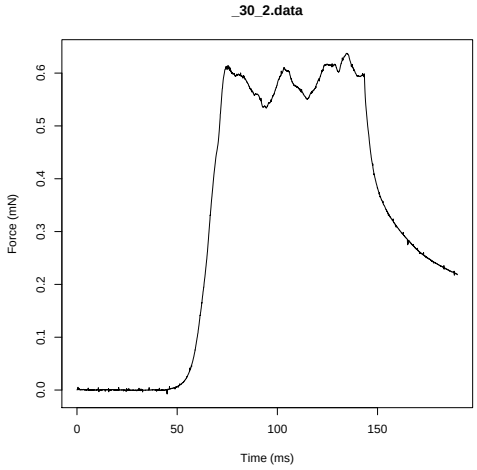

Figure 3.8: $-30°$ Pattern Trial 2

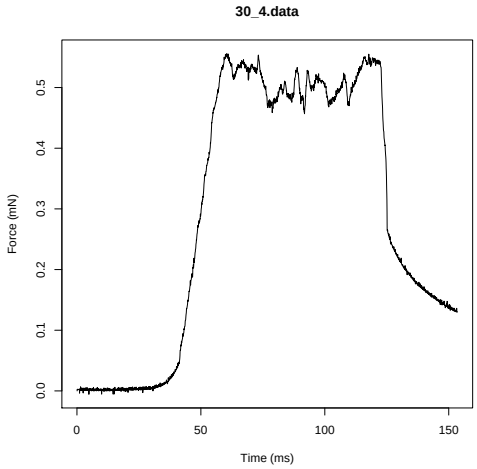

Figure 3.9: $30°$ Pattern Trial 1

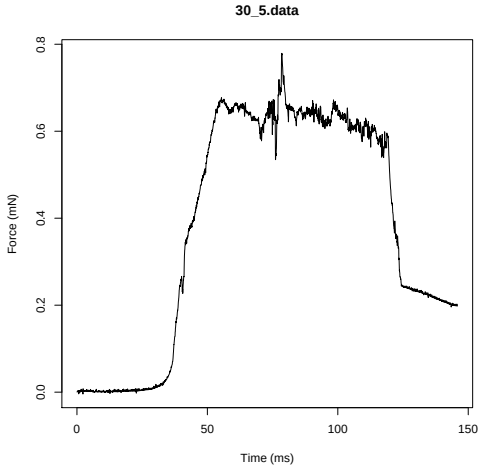

Figure 3.10: 30° Pattern Trial 2

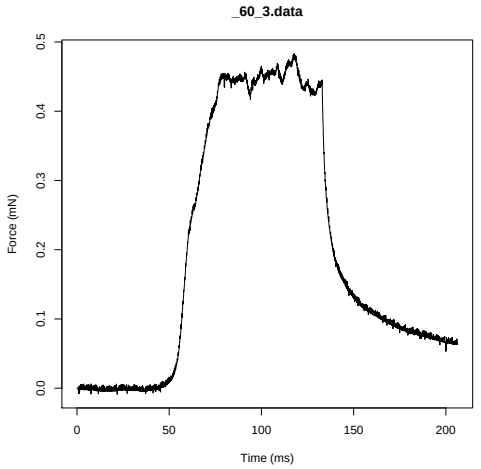

Figure 3.11: −60° Pattern Trial 1

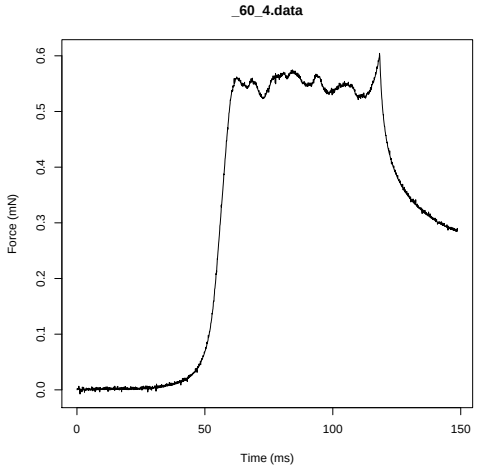

Figure 3.12: $-60°$ Pattern Trial 2

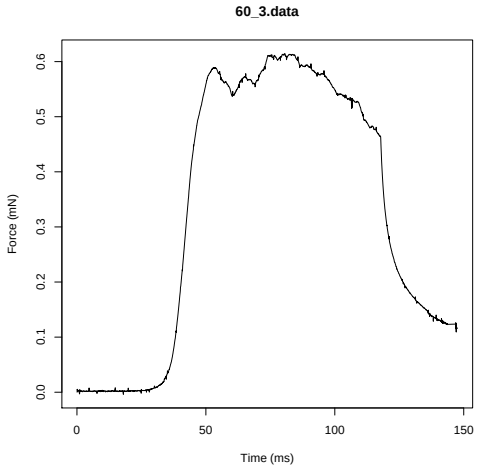

Figure 3.13: $60°$ Pattern Trial 1

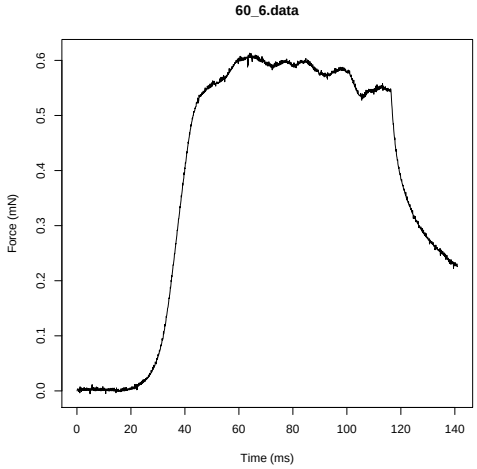

Figure 3.14: 60° Pattern Trial 2

Curved Pattern

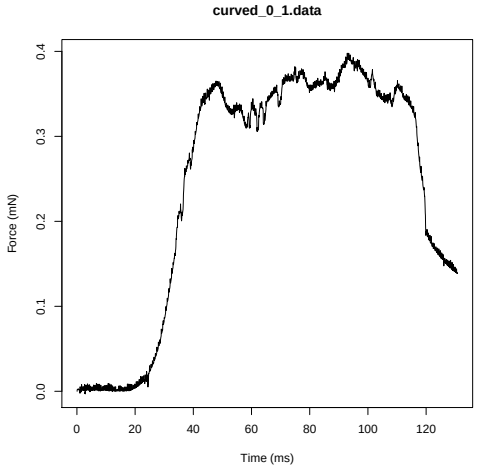

Figure 3.15: Curved Pattern Orientation 0 Trial 1

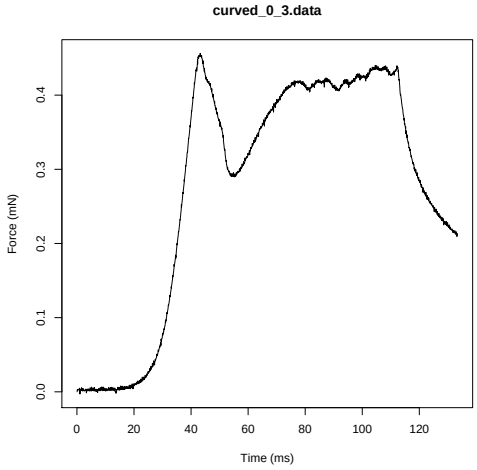

Figure 3.16: Curved Pattern Orientation 0 Trial 2

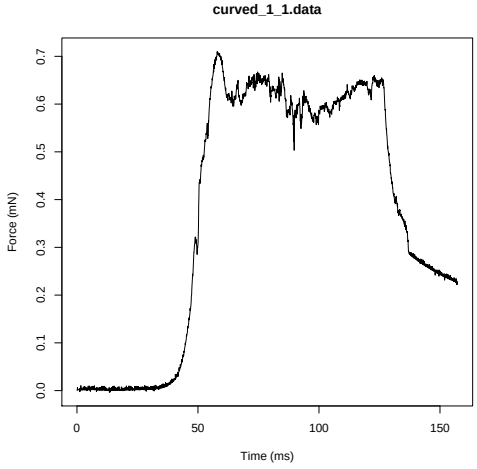

Figure 3.17: Curved Pattern Orientation 1 Trial 1

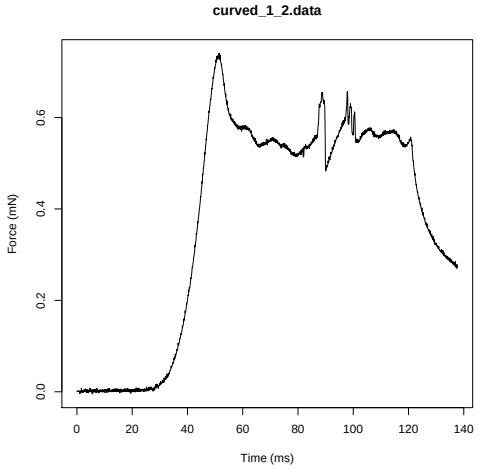

Figure 3.18: Curved Pattern Orientation 1 Trial 2

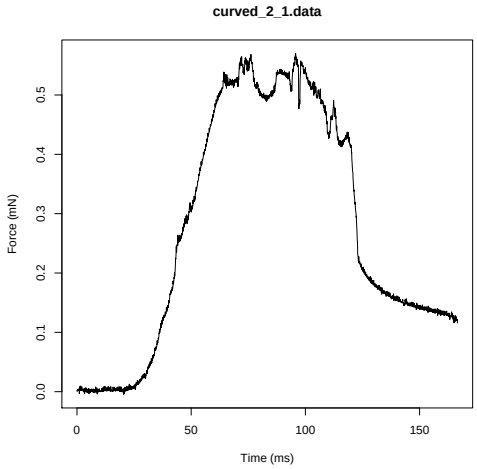

Figure 3.19: Curved Pattern Orientation 2 Trial 1

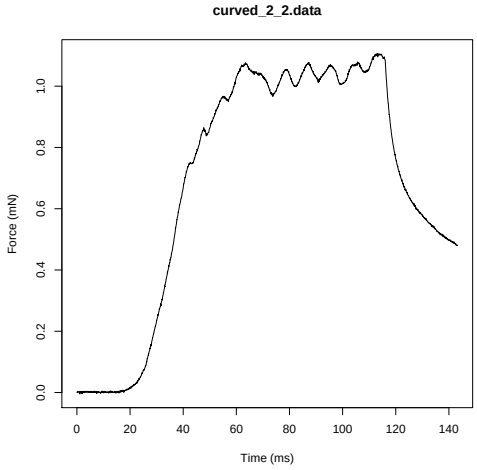

Figure 3.20: Curved Pattern Orientation 2 Trial 2

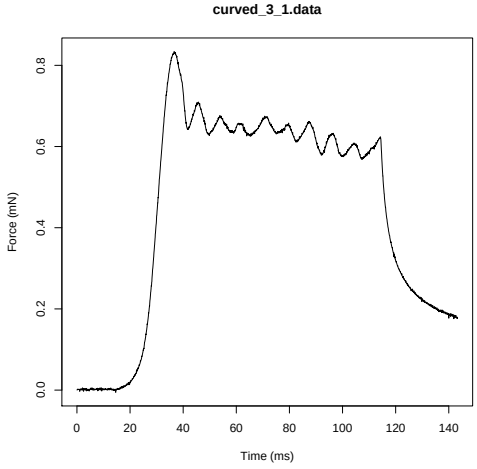

Figure 3.21: Curved Pattern Orientation 3 Trial 1

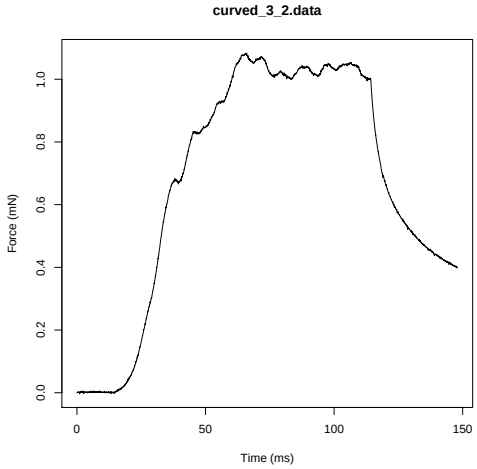

Figure 3.22: Curved Pattern Orientation 3 Trial 2

Random Pattern

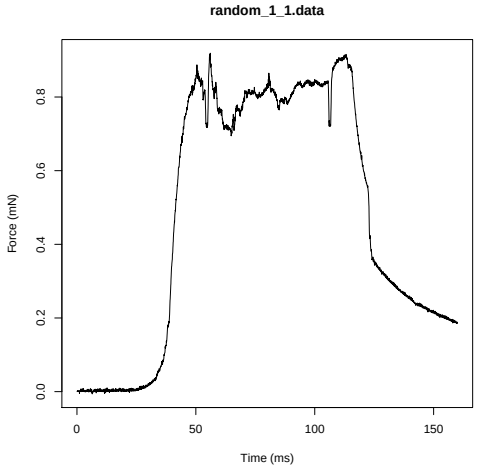

Figure 3.23: Random Pattern Trial 1

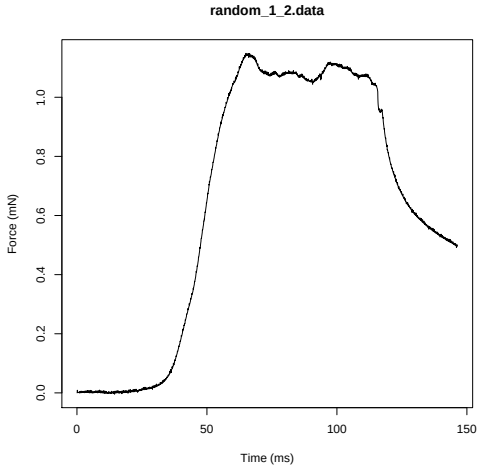

Figure 3.24: Random Pattern Trial 2

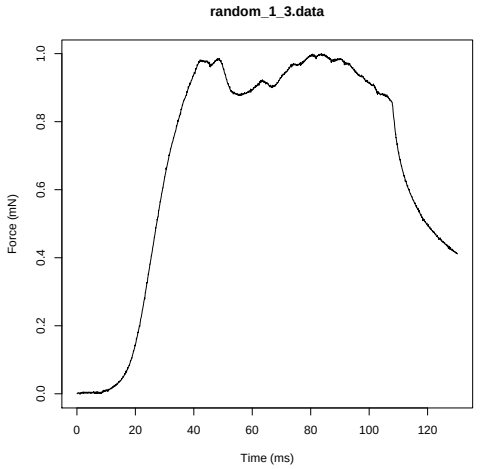

Figure 3.25: Random Pattern Trial 3

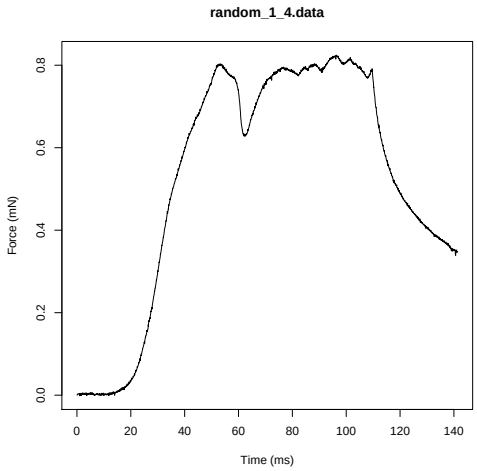

Figure 3.26: Random Pattern Trial 4

3.1.2 Discussion

As one would expect, in Figures 3.1 and 3.2, one can see that the force climbs steeply and stays roughly constant for the duration of the peeling. This should be the baseline, as this peeling experiment was carried out with no pattern at all, only a transparency.

In Figures 3.3 and 3.4, one can see that the force regularly oscillates, suggesting that the force required to keep the tape peeling at a constant rate increases when the tape encounters a line of ink parallel to the peel front. This makes sense since all points on the peel front are affected equally.

In Figures 3.5 and 3.6, one can see that the force profile is analogous to the homogeneous case. The force climbs quickly and stays relatively constant for the duration of the peeling.

In Figures 3.7 to 3.14, one can see that, like the horizontal case and unlike the vertical case, the force varies quite regularly, increasing whenever a part of the front encounters a line of the pattern, although the oscillation in force is less than in the horizontal case.

In Figures 3.15 to 3.22, one can see the anisotropic response of the tape to the pattern. The force required in some configurations is less than in other configurations, despite the pattern being the same.

Finally, in Figures 3.23 to 3.26, one can see that a random pattern produces a different output every time due to the fact that the placement of the tape on the pattern is different every time.

With all of these different patterns tested, it is useful to compare the peak force for each pattern against the homogeneous "pattern"'s peak force. These values are listed in Table 3.1.

Pattern	Peak Force (mN) (Trial 1, Trial 2)
Homogeneous	1.39722595, 1.35711272
Vertical	0.50075887, 0.56532128
Horizontal	0.48564452, 0.51067015
30°	0.55595294, 0.77913889
60°	0.61453621, 0.61322550
−30°	0.56490604, 0.63745234
−60°	0.48322745, 0.60448711

Table 3.1: Peak Forces for different patterns

3.2 Computational Results

3.2.1 Results

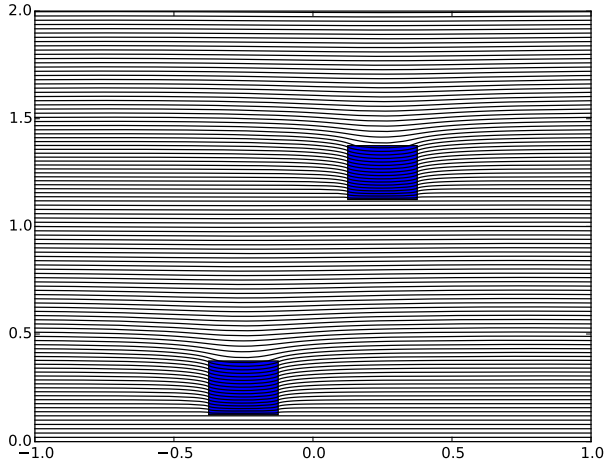

Figure 3.27: $G_\infty = 1$, amp $= 1$

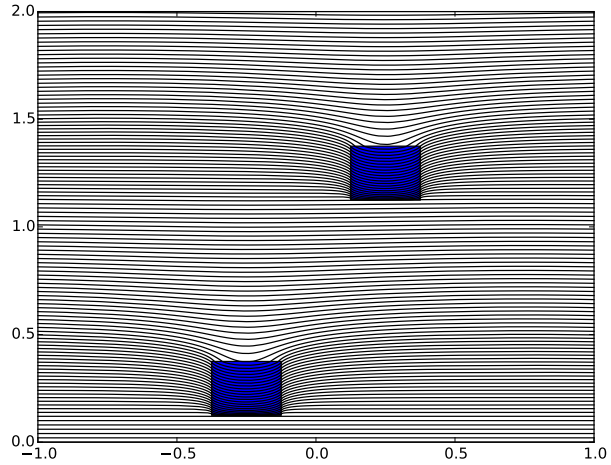

Figure 3.28: $G_\infty = 1$, amp $= 2$

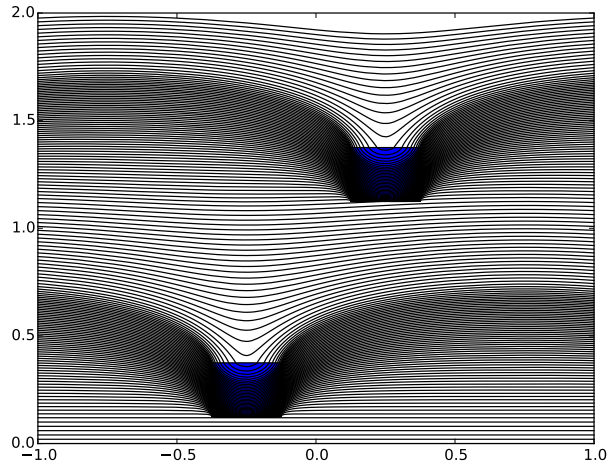

Figure 3.29: $G_\infty = 1$, amp $= 5$

		G_∞			
		1	2	5	10
A	1	2.0825	2.2243	3.2382	∞
	2	1.0178	1.0413	1.1611	1.6191
	5	0.4026	0.40551	0.41648	0.44484
	10	0.20064	0.20131	0.20355	0.20825

Table 3.2: Convergence Times (seconds)

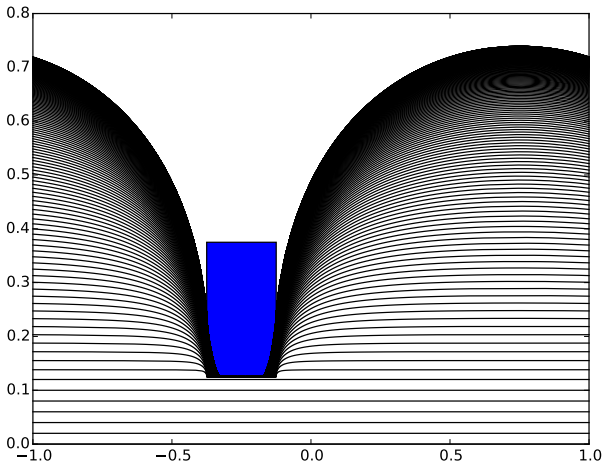

Figure 3.30: $G_\infty = 1$, amp $= 10$

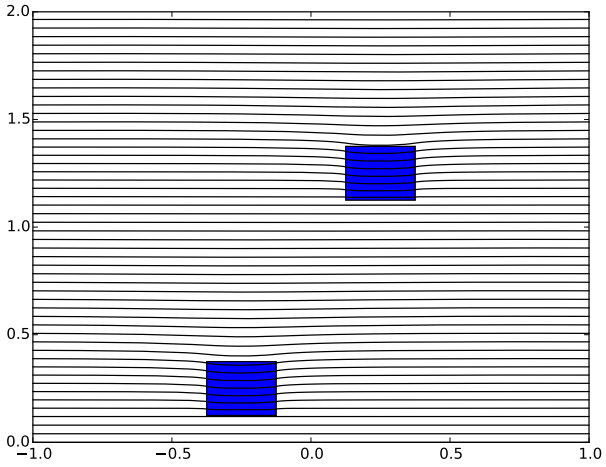

Figure 3.31: $G_\infty = 2$, amp $= 1$

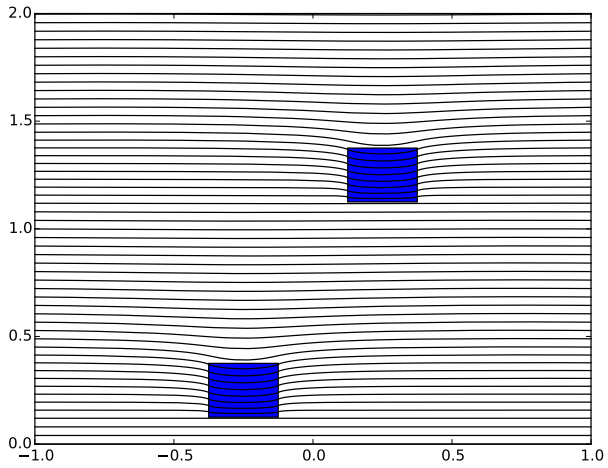

Figure 3.32: $G_\infty = 2$, amp $= 2$

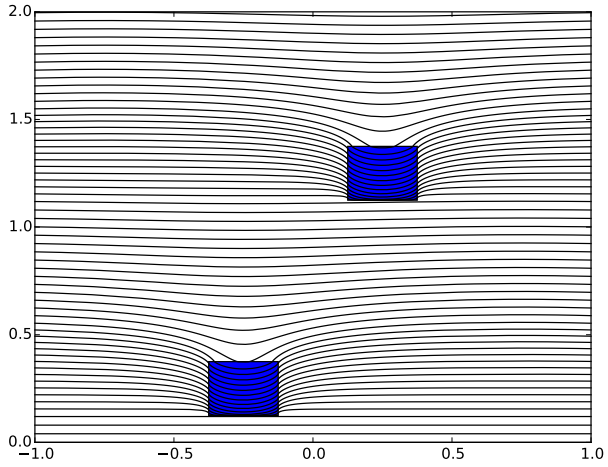

Figure 3.33: $G_\infty = 2$, amp $= 5$

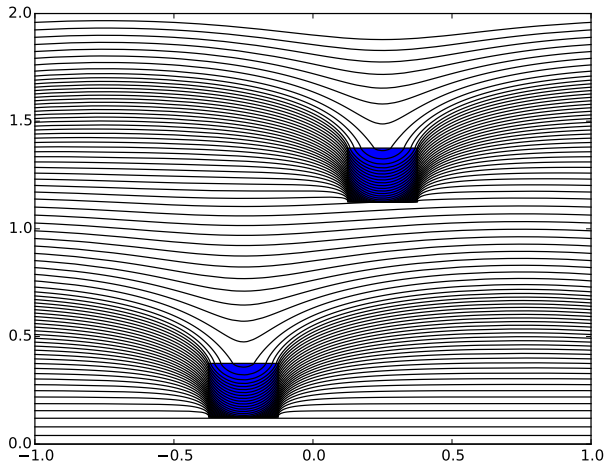

Figure 3.34: $G_\infty = 2$, amp $= 10$

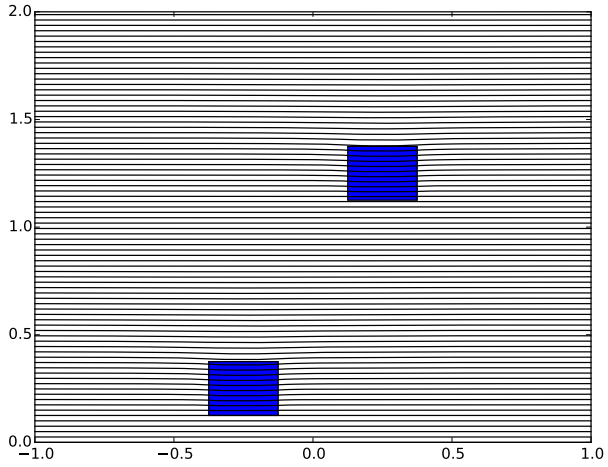

Figure 3.35: $G_\infty = 5$, amp $= 1$

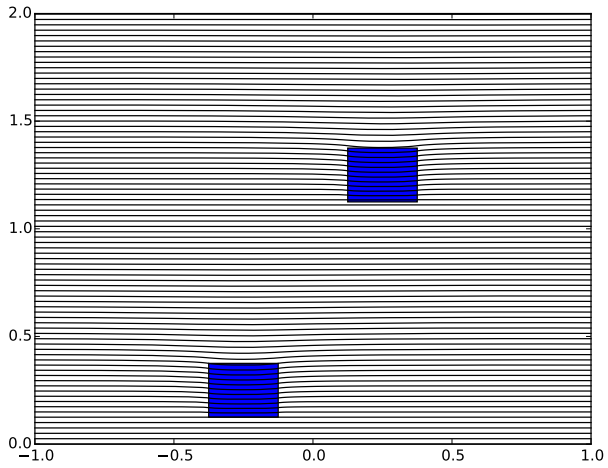

Figure 3.36: $G_\infty = 5$, amp $= 2$

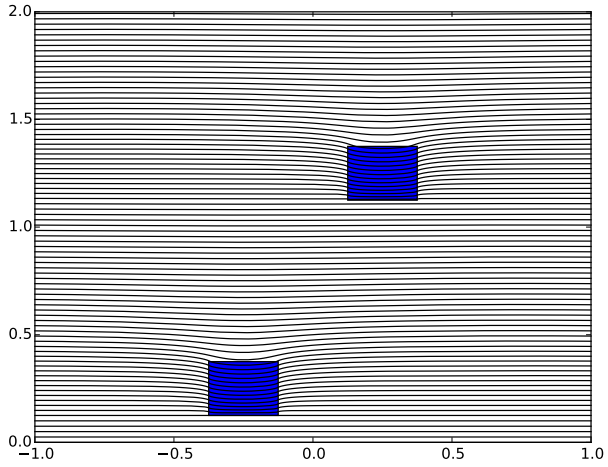

Figure 3.37: $G_\infty = 5$, amp $= 5$

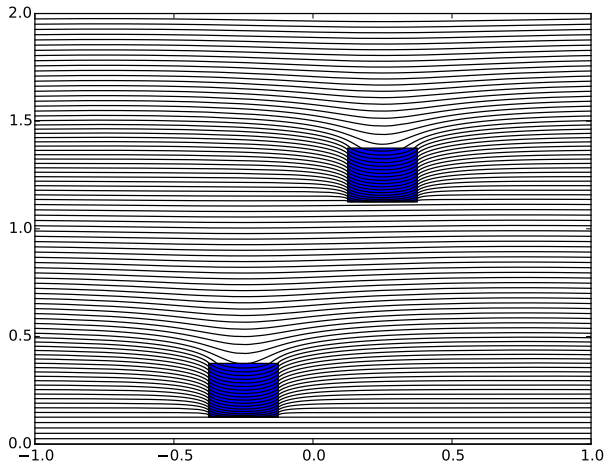

Figure 3.38: $G_\infty = 5$, amp $= 10$

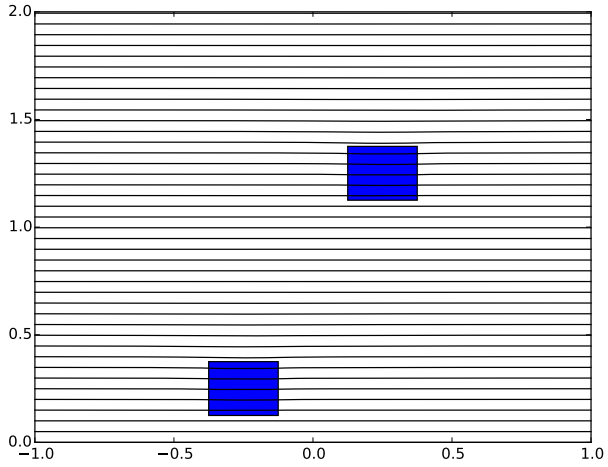

Figure 3.39: $G_\infty = 10$, amp $= 1$

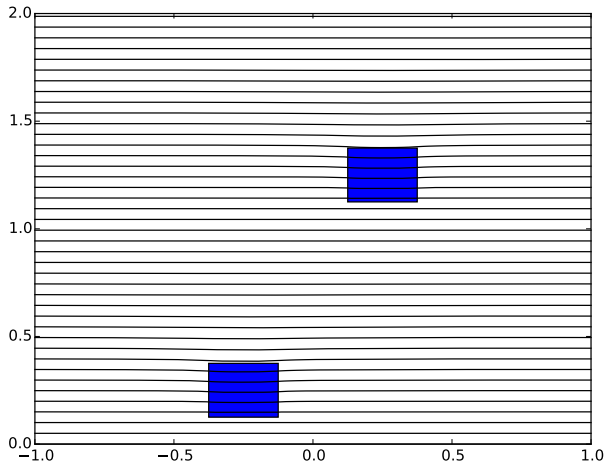

Figure 3.40: $G_\infty = 10$, amp $= 2$

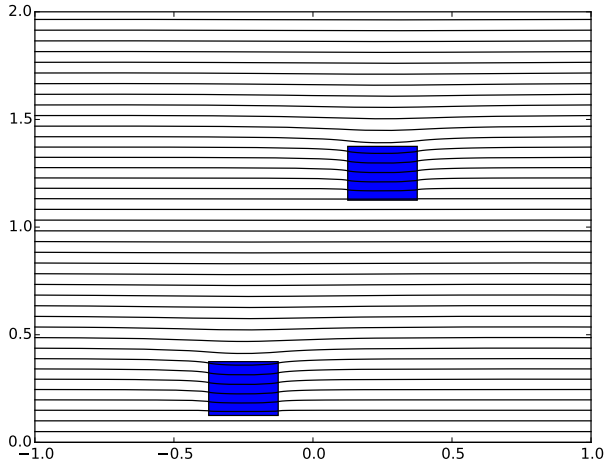

Figure 3.41: $G_\infty = 10$, amp $= 5$

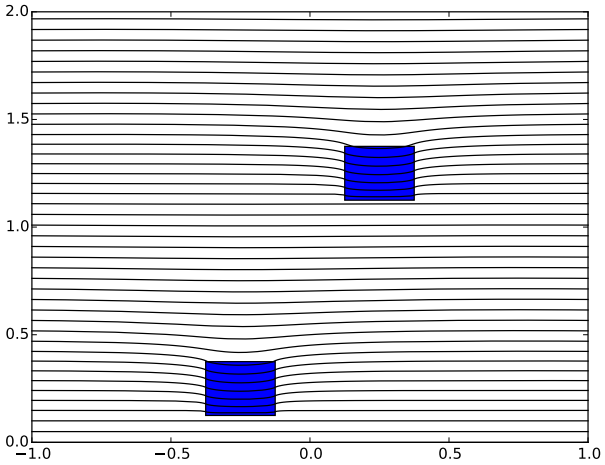

Figure 3.42: $G_\infty = 10$, amp $= 10$

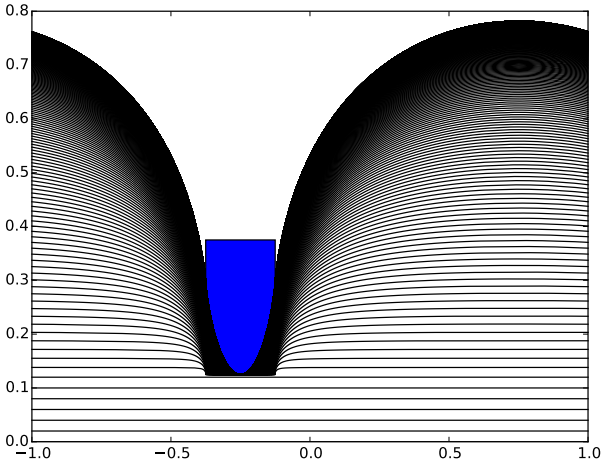

Figure 3.43: $G_\infty = 1$, amp $= 8$

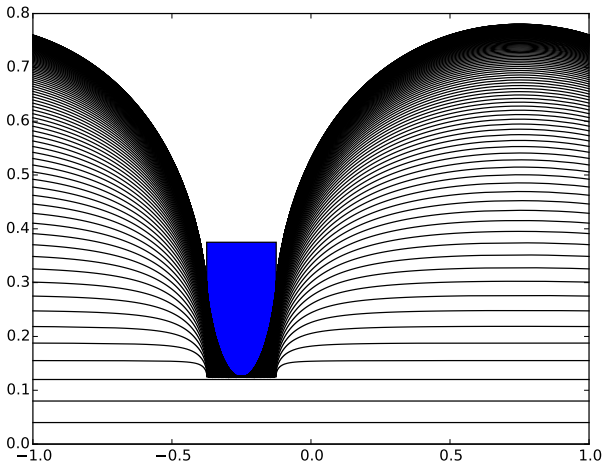

Figure 3.44: $G_\infty = 2$, amp $= 16$

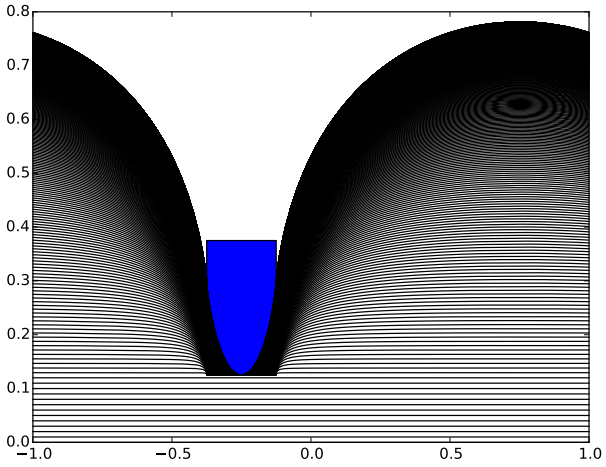

Figure 3.45: $G_\infty = 5$, amp $= 40$

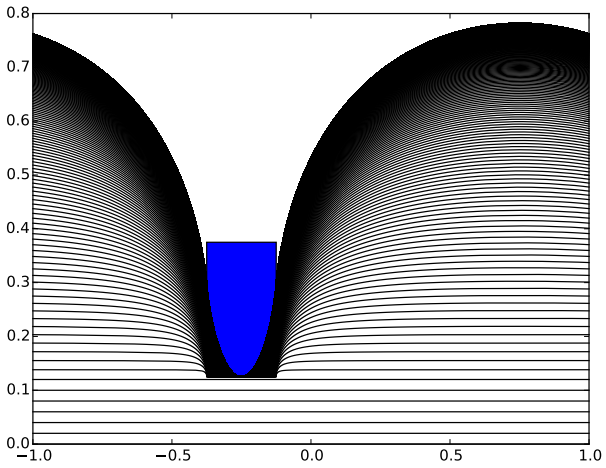

Figure 3.46: $G_\infty = 10$, amp $= 80$

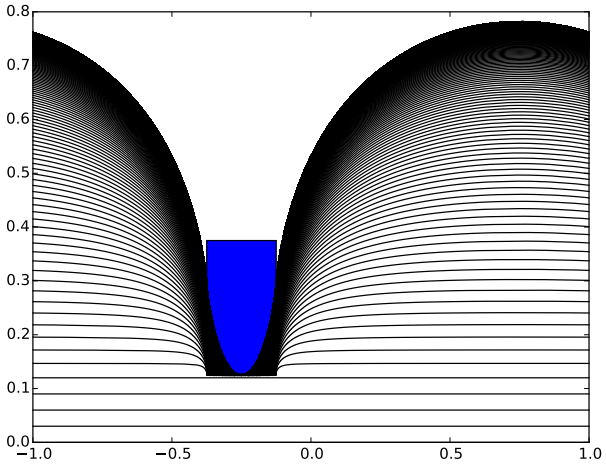

Figure 3.47: $G_\infty = 15$, amp $= 120$

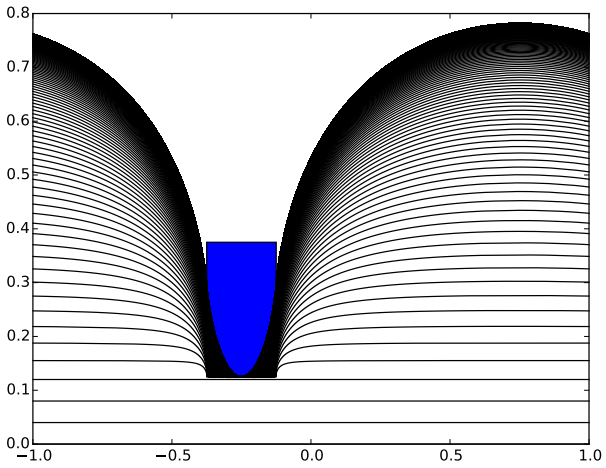

Figure 3.48: $G_\infty = 20$, amp $= 160$

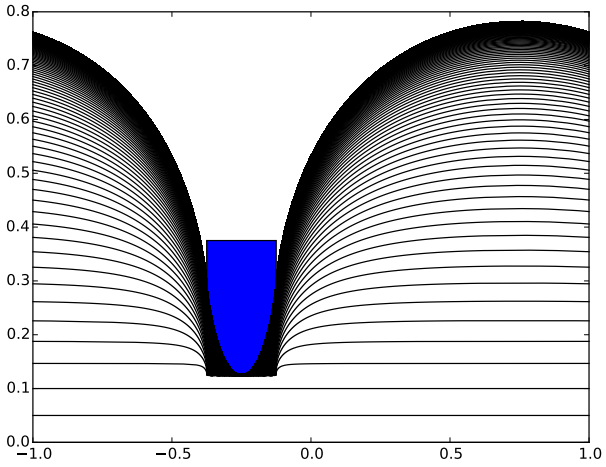

Figure 3.49: $G_\infty = 25$, amp $= 200$

G_∞	A_c
1	8
2	16
5	40
10	79
15	120
20	160
25	200

Table 3.3: Critical A for each G_∞

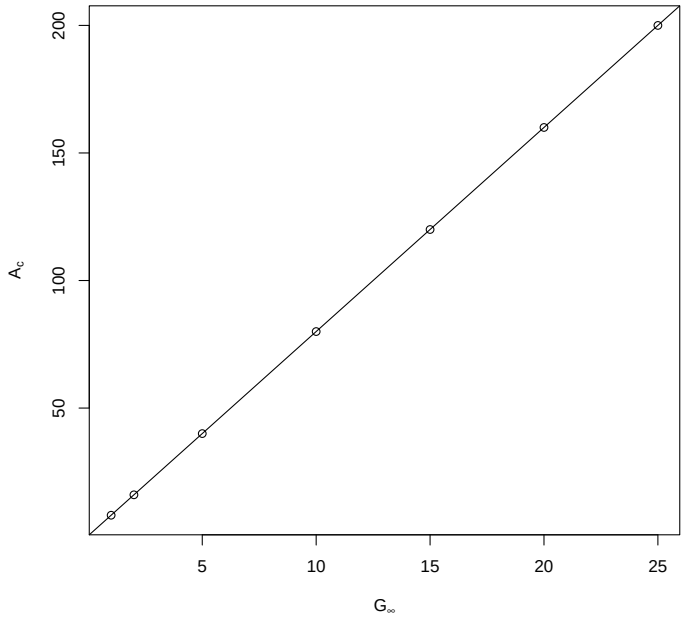

Figure 3.50: Correlation between G_∞ and A_c

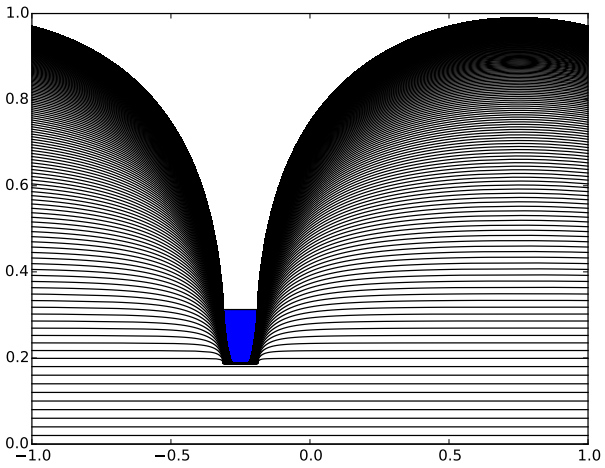

Figure 3.51: $A_c = 18$ for square size of 0.125

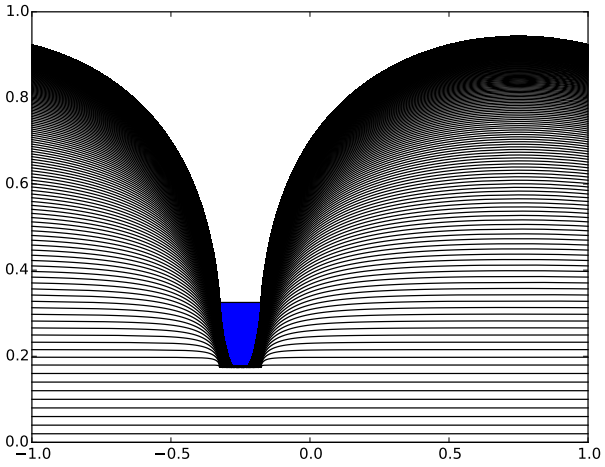

Figure 3.52: $A_c = 14$ for square size of 0.15

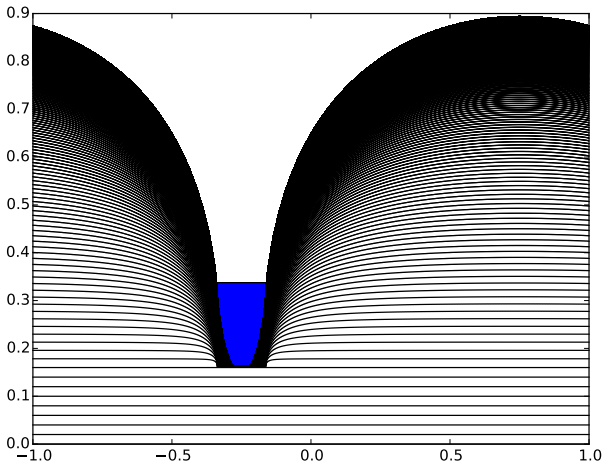

Figure 3.53: $A_c = 12$ for square size of 0.175

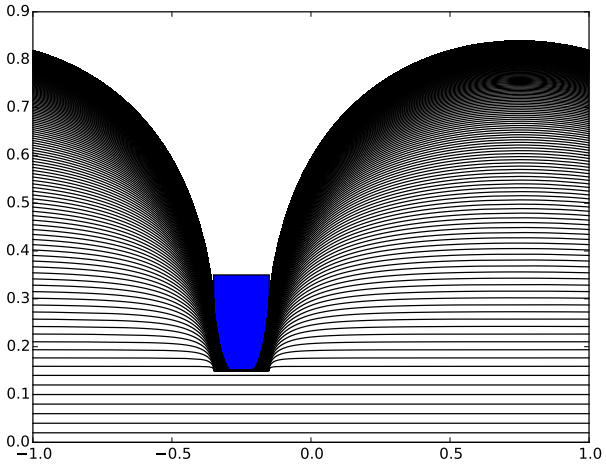

Figure 3.54: $A_c = 11$ for square size of 0.2

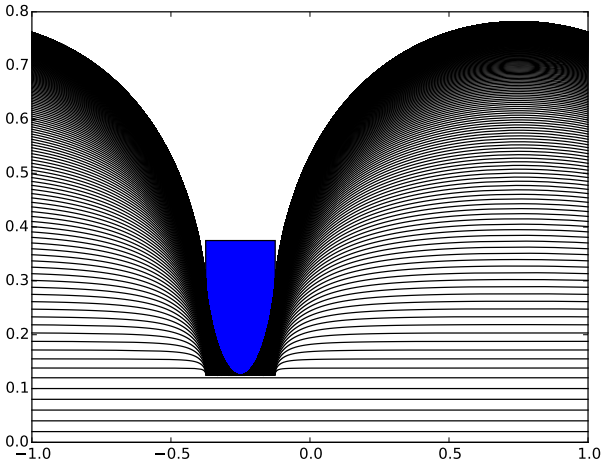

Figure 3.55: $A_c = 8$ for a square size of 0.25

Square Size	A_c
0.125	18
0.15	14
0.175	12
0.20	11
0.25	8

Table 3.4: Critical A for $G_\infty = 1$ for each square size

3.2.2 Discussion

First, a candidate set of G_∞ and A was investigated. The G_∞ that were initially investigated were 1, 2, 5, and 10. The A that were initially investigated were 1, 2, 5, and 10 as well. These results can be seen in Figures 3.27 to 3.42. The convergence times are recorded in Table 3.2. The fact that the case $G_\infty = 1$, $A = 10$ did not terminate was intriguing and raised the question as to whether there is a relation between G_∞ and A_c, that is, the critical A such that the peel front gets stuck. Thus, the same G_∞ were investigated, but simulations were done until the critical A_c was found. These are listed in Table 3.3. These were then plotted in Figure 3.50 and a line of best fit was found. This line was shown to be $A_c = 8G_\infty$,

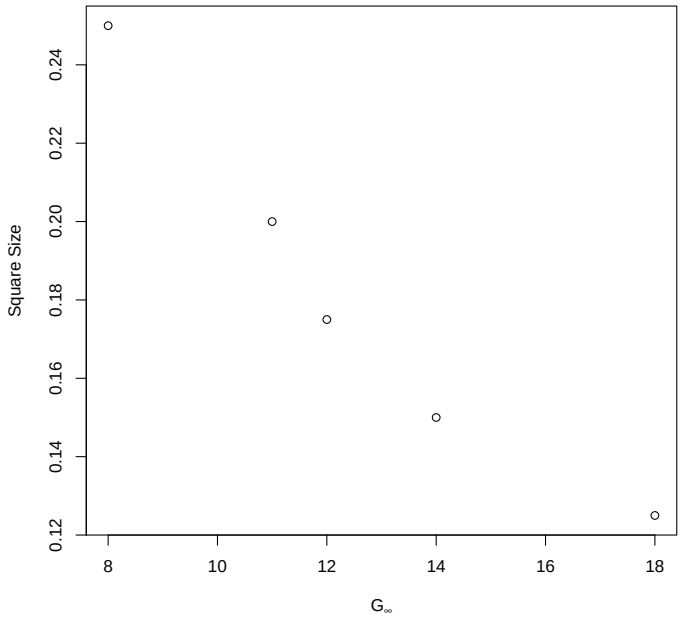

Figure 3.56: Correlation between square size and A_c

or $G_\infty = \frac{1}{8}A_c$, or $\frac{G_\infty}{A_c} = \frac{1}{8}$.

Once this was shown for one pattern, it is natural to investigate if the value of A_c depends at all on the pattern. One of the first criteria that comes to mind is the size of the pattern. Thus, the value of $G_\infty = 1$ was selected to keep everything simple and A_c was investigated for many different pattern sizes. This is shown in Figures 3.51 to 3.55. The relationship between square size and A_c is shown in Table 3.4 and Figure 3.56. It is interesting to note that there is a inverse relationship between square size and A_c, which intuitively makes sense. If the pattern area is smaller, then the force exerted by each point in that area must be larger to account for the smaller area of peel front affected by it.

This extremely perfect relationship between G_∞ and A_c must have some root in the equation, so it is instructive to work with the peel front equation to arrive at a formula for the parameter in question. First, we have the peel front equation (Equation (3.1)). Initially, $G\left(x, f\left(x,t\right)\right)$ is a function that can return either 0 or A. By extracting an A out of G

(Equation (3.2)), we convert G into a function that returns 0 or 1. This allows us to play with A explicitly. We then divide everything by A (Equation (3.3)). When the peel front gets stuck, $\frac{\partial \hat{f}}{\partial t} = 0$. We are therefore trying to find the minimum A for a certain G_∞ such that $\frac{\partial \hat{f}}{\partial t} = 0$. Equation (3.6) shows the resulting equation when solved for $\frac{G_\infty}{A_c}$. If $\frac{G_\infty}{A_c}$ is a constant (for a given $G(x, f(x,t))$), it means there is a direct relationship between the Fourier transform of $G(x, f(x,t))$ and $1 - 4|k|\hat{f}(k,t)$. In addition, from the second set of results, it is clear that as the area of the squares is decreased, the critical amplification factor is higher. From this, it is clear that the ratio between $\mathcal{F}[G(x, f(x,t))]$ and $1 - 4|k|\hat{f}(k,t)$ becomes smaller as the area of the squares decreases.

$$\frac{\partial \hat{f}}{\partial t}(k,t) = -c|k|\hat{f}(k,t) + \mathcal{F}[G_\infty - G(x, f(x,t))] \tag{3.1}$$

$$\frac{\partial \hat{f}}{\partial t}(k,t) = -c|k|\hat{f}(k,t) - A\mathcal{F}[G(x, f(x,t))] + G_\infty \tag{3.2}$$

$$\frac{1}{A}\frac{\partial \hat{f}}{\partial t}(k,t) = -\frac{4G_\infty}{A}|k|\hat{f}(k,t) - \mathcal{F}[G(x, f(x,t))] + \frac{G_\infty}{A} \tag{3.3}$$

$$\frac{1}{A}\frac{\partial \hat{f}}{\partial t}(k,t) = \frac{G_\infty}{A}\left(1 - 4|k|\hat{f}(k,t)\right) - \mathcal{F}[G(x, f(x,t))] \tag{3.4}$$

$$0 = \frac{G_\infty}{A}\left(1 - 4|k|\hat{f}(k,t)\right) - \mathcal{F}[G(x, f(x,t))] \tag{3.5}$$

$$\frac{G_\infty}{A_c} = \frac{\mathcal{F}[G(x, f(x,t))]}{1 - 4|k|\hat{f}(k,t)} \tag{3.6}$$

Chapter 4

Conclusion

In conclusion, it can be seen that there is a strong correlation between the variations in the applied force and certain types of regular patterns. The theoretical model was verified by the experimental results. Furthermore, the computational results show a surprising relationship between the constant driving force G_∞ and the critical amplification factor beyond which the peel front gets stuck. It was also shown that this relationship depends inversely on the size of the square patches. These effects further related two quantities in the peel front equation which may, with further work, help predict the shape of the peel front for certain $G\left(x, f\left(x,t\right)\right)$. These effects should be further explored to examine their possible predictive powers.

Bibliography

[1] B. Craciun and K. Bhattacharya. "Effective motion of a curvature-sensitive interface through a heterogeneous medium". In: *Interface Free Bound* 6.2 (2004), pp. 151–173.

[2] N. Dirr and N. Yip. "Pinning and de-pinning phenomena in front propagation in heterogeneous media". In: *Interface Free Bound* 8.1 (2006), pp. 79–109.

[3] P. Dondl and K. Bhattacharya. "A sharp interface for the propagation of martensitic phase boundaries". In: *Arch. Ration. Mech. An.* 197 (2010), pp. 599–617.

[4] L. Legrand et al. "Coplanar perturbation of a crack lying on the mid-plane of a plate". In: *International Journal of Fracture* 170 (2011), pp. 67–82.

[5] J. R. Rice. "1st-order variation in elastic fields due to variation in location of a planar crack front". In: *Journal of Applied Mechanics – Transactions of the ASME* 52.3 (1985), pp. 571–579.

[6] R. S. Rivlin. "The effective work of adhesion". In: *Paint Technology* 9 (1944), p. 215.

[7] S. M. Xia et al. "Adhesion of heterogeneous thin films—I: Elastic heterogeneity". In: *Journal of the Mechanics and Physics of Solids* (2013).

[8] S. M. Xia et al. "Adhesion of heterogeneous thin films—II: Adhesive heterogeneity". In: *Journal of the Mechanics and Physics of Solids* (2014).

[9] S. Xia et al. "Toughening and Asymmetry in Peeling of Heterogeneous Adhesives". In: *Physical Review Letters* (2012).